doi: **10.12029/gc20160421**

李志丹, 陈军强, 王佳营, 等. 内蒙古达茂旗宫忽洞矽卡岩型铜矿床地质、地球化学特征及其意义[J]. 中国地质, 2016, 43(4): 1367−1384.
Li Zhidan, Chen Junqiang, Wang Jiaying, et al. Geology and geochemistry of the Gonghudong skarn copper deposit in Darhan Muminggan Joint Banner, Inner Mongolia and its significance[J]. Geology in China, 2016, 43(4): 1367−1384(in Chinese with English abstract).

内蒙古达茂旗宫忽洞矽卡岩型铜矿床地质、地球化学特征及其意义

李志丹 陈军强 王佳营 文思博 肖志斌 汤 超 刘 行 俞礽安

（中国地质调查局天津地质调查中心 非化石能源矿产实验室, 天津 300170）

提要：宫忽洞是内蒙古中部的一例典型矽卡岩型铜矿床，位于华北板块北缘中段中元古代白云鄂博裂谷带内，赋存于矿区东南部花岗斑岩与白云鄂博群呼吉尔图组结晶灰岩形成的矽卡岩中。矿体呈透镜状、似层状分布，主要金属矿物为黄铜矿、斑铜矿、闪锌矿、辉铜矿、黄铁矿、磁黄铁矿等，脉石矿物为石榴石、透辉石、方解石、萤石等，矽卡岩类主要为透辉石−石榴石矽卡岩。花岗斑岩LA−ICP−MS锆石U−Pb年龄为(299.6±1.7) Ma，推断宫忽洞铜矿床是晚古生代构造岩浆活动的产物。花岗斑岩高Si、贫Al；亏损Ba、Sr、P、Ti等元素；10000Ga/Al值变化于2.32~3.49；稀土配分曲线呈典型的“V”字形；FeO^T/MgO值介于9.86~12.27；其成因类型为A1亚类的A型花岗岩，可能形成于后造山拉张构造环境。3件热液方解石$\delta^{13}C_{V-PDB}$值介于−10.6‰~−8.6‰，对应的$\delta^{18}O_{V-SMOW}$值为4.6‰~15‰，宫忽洞铜矿床成矿期的CO_2可能由花岗斑岩与灰岩地层的相互作用形成。4件不同硫化物的$\delta^{34}S$值介于1.2‰~10‰，表明成矿所需的硫可能来自于岩浆硫与海相硫酸盐的混合；4件不同硫化物的$^{206}Pb/^{204}Pb$=17.706~17.828，$^{207}Pb/^{204}Pb$=15.506~15.564；$^{208}Pb/^{204}Pb$=37.841~37.969，表明后造山阶段拉张环境形成的A型花岗斑岩体可能是成矿物质的主要提供者。

关 键 词：矿床地质；矿床地球化学；矽卡岩型铜矿床；宫忽洞；达茂旗

中图分类号：P618.41；P597 **文献标志码**：A **文章编号**：1000−3657(2016) 04−1367−18

Geology and geochemistry of the Gonghudong skarn copper deposit in Darhan Muminggan Joint Banner, Inner Mongolia and its significance

LI Zhi−dan, CHEN Jun−qiang, WANG Jia−ying, WEN Si−bo, XIAO Zhi−bin, TANG Chao, LIU Xing, YU Reng−an

（*Laboratory of Non−fossil Energy Minerals, Tianjin Center of China Geological Survey, Tianjin* 300170*, China*）

Abstract: The Gonghudong is a typical skarn copper deposit in central Inner Mongolia. It is located in Mesoproterozoic Bayan Obo rift zone along the middle section of the northern margin of North China plate, and is hosted in the skarn belt formed by the contact

收稿日期：2015−07−25；**改回日期**：2015−12−30

基金项目：中国地质调查项目（12120113057300、12120113057400）和国家自然科学基金项目（41502082）联合资助。

作者简介：李志丹，男，1986年生，硕士，工程师，矿床学、矿产普查与勘探专业；E−mail：cugcug@qq.com。

of granite porphyry and crystalline limestone of Hujiertu Group. The Cu orebodies are lentoid and stratiform-like in shape. The metallic minerals mainly are chalcopyrite, bornite, sphalerite, chalcocite, pyrite and pyrrhotine, and the nonmetallic minerals mainly are garnet, diopside, calcite and fluorite. The LA-ICP-MS zircon U-Pb dating of granite porphyry yielded an age of (299.6±1.7) Ma, and thus the Gonghudong deposit was the product of Late Paleozoic tectonic magmatic activity. The granite porphyry has high Si, low Al, depleted Ba, Sr, P, Ti, with "V" type REE pattern, and the values of 10000Ga/Al and FeO^T/MgO range from 2.32 to 3.49 and 9.86 to 12.27, respectively. These data indicate that the granite porphyry belongs to A1 subtype of A-type granites and was formed in a post-orogenic extension environment. $\delta^{13}C_{V-PDB}$ and $\delta^{18}O_{V-SMOW}$ of the hydrothermal calcite are from −10.6‰ to −8.6‰ and from 4.6‰ to 24.67‰, respectively, suggesting that the CO_2 was supplied by the interaction of granite porphyry and limestone. The $\delta^{34}S$ values of the sulfide range from 1.2‰ to 10‰, indicating that the sulfur was derived from the magma sulfur and marine sulfate. $^{206}Pb/^{204}Pb$, $^{207}Pb/^{204}Pb$ and $^{208}Pb/^{204}Pb$ of the ores are 17.847 to l8.173, 15.586 to 15.873 and 37.997 to 38.905, respectively. The Pb-isotopic compositions suggest that the ore-forming material was probably derived mainly from the granite porphyry.

Key words: ore geology; geochemistry; skarn copper deposit; Gonghudong, Darhan Muminggan Joint Banner

About the first author: LI Zhi-dan, male, born in 1986, master, engineer, engages in the study of ore geology and exploration; E-mail: cugcug@qq.com.

Fund support: Supported by China Geological Survey Program (No. 12120113057300, No. 12120113057400), National Natural Science Foundation of China (No. 41502082).

中蒙边境相邻区是重要的斑岩型铜、金矿床分布区[1-4],境外产出有欧玉陶勒盖(Oyu Tolgoi)和查干苏布尔加(Tsagaan Suvarga)等特大型矿床[5-6],境内也陆续在新疆阿勒泰南缘、东天山、甘肃北山、二连—东乌旗等地区取得了较好的找矿效果[7-10]。内蒙古达茂旗地处中蒙边境中段,临近索伦山蛇绿混杂岩带,是斑岩型铜(金)矿床找矿的理想地区[4],近年来该区陆续发现了查干诺尔、善丹、沙尔陶勒盖、哈布齐尔等一批矿产地[11-13],指示出较好的找矿前景。内蒙古达茂旗宫忽洞是一例与花岗斑岩相关的典型矽卡岩型铜矿床。矽卡岩型矿床作为斑岩成矿系统的重要组成,对此类矿床开展典型矿床研究对区内成矿与找矿研究意义重大[14-16]。该矿床位于达茂旗百灵庙镇北东约9 km处,发现于20世纪50年代,目前保有铜金属量1.6万t,平均品位为0.99%[17]。自发现以来,宫忽洞铜矿还未开展过系统的研究工作,与成矿相关的花岗斑岩的时代、成因类型、构造环境等尚不清楚,而相关成矿物质的来源亦不明确。本文在前人地质勘查的基础上,描述了宫忽洞铜矿床的地质特征,并对矿区南部花岗斑岩开展了年代学、岩石地球化学研究,对矿石矿物进行了硫、铅同位素组成、对热液方解石进行了碳、氧同位素地球化学研究,以期对成矿作用有所认识。

1 区域地质特征

宫忽洞铜矿床位于华北板块北缘中段中元古代白云鄂博裂谷带内,其北接温都尔庙俯冲增生杂岩带,南邻色尔腾山—太仆寺旗古岩浆弧(图1-A)。白云鄂博裂谷带是中元古代时期在乌拉山岩群和色尔腾山岩群组成的基底上发展而成的大型裂谷带,东西长约800 km,南北宽20~50 km[18],裂谷带内沉积白云鄂博群沉积-火山岩,主要岩石类型有石英岩、细砂岩、石英砂岩、灰岩、砂质板岩、泥质粉砂岩和碳质板岩,局部地段见有粗面岩、英安岩和流纹岩,整套岩层厚度为9000 m[19],是白云鄂博铁-铌-稀土矿、浩尧尔忽洞金矿、赛乌素金矿、翁公山铁矿的容矿主岩。

宫忽洞铜矿区域内主要出露白云鄂博群白音宝拉格组(Qnb^4)四段;呼吉尔图组一段(Qnh^1)、二段(Qnh^2)、三段(Qnh^3);阿牙登组(Qna);其次为下二叠统苏吉火山岩(sv)、白垩系固阳组(K_1g)、二连组(K_2e)和第三系汉诺坝组(N_1h)(图1-B)。其中,白音宝拉格组(Qnb^4)四段岩性为暗灰色绢云母板岩及灰白色变质中粗粒石英砂岩;呼吉尔图组一段(Qnh^1)为灰色藻席纹层灰岩及粉晶灰岩;二段(Qnh^2)为暗灰色钙硅角岩与阳起石角岩互层夹变质硅质泥岩;三段(Qnh^3)为灰黑色泥岩及粉砂岩夹

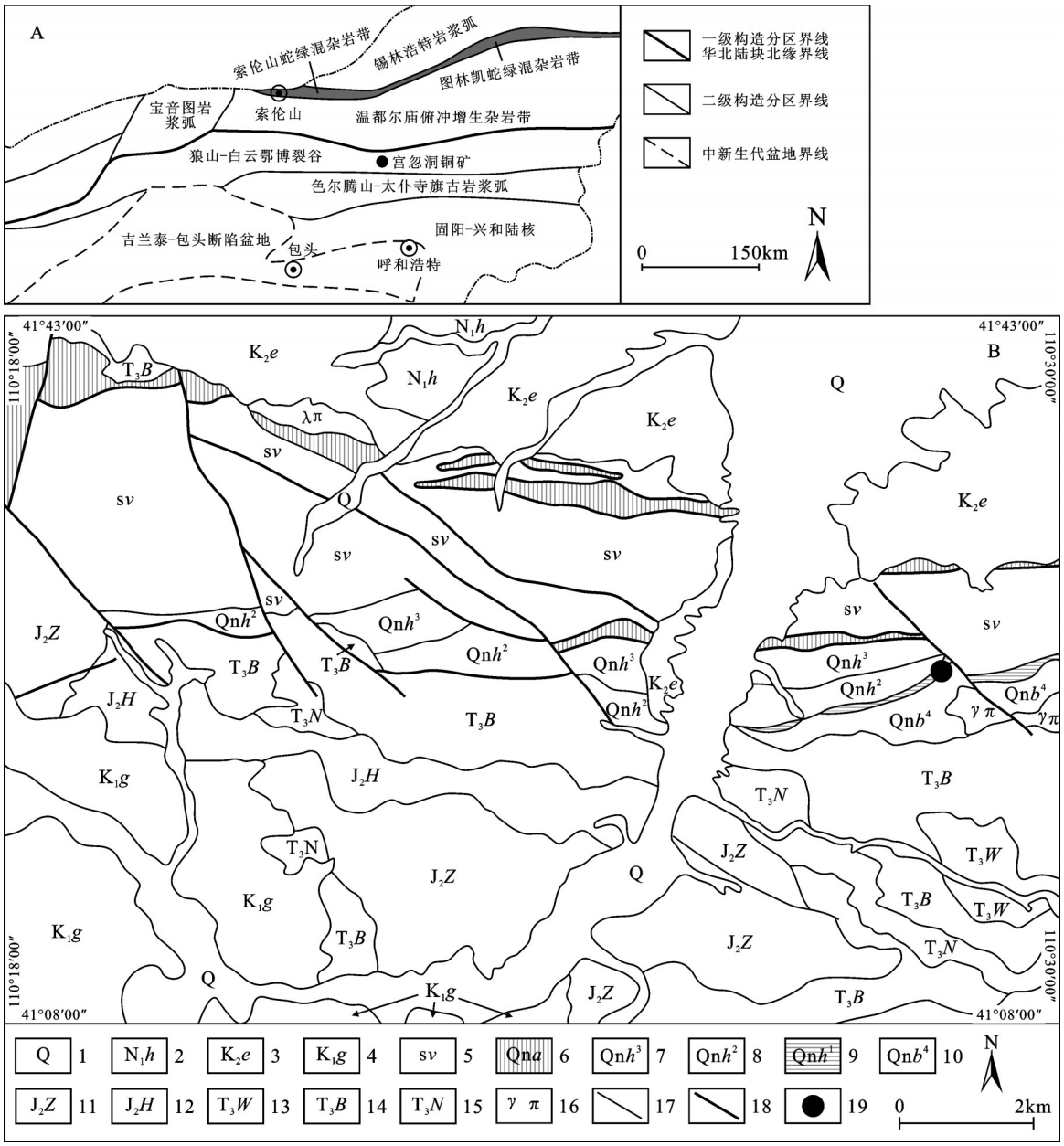

图1 内蒙古达茂旗宫忽洞铜矿床大地构造位置(A)及区域地质图(B)(A—引自文献[21];B—引自文献[20])

1—第四系;2—汉诺坝组;3—二连组;4—固阳组;5—苏吉火山岩;6—阿牙登组;7—呼吉尔图组三段;8—呼吉尔图组二段;9—呼吉尔图组一段;10—白音宝拉格组四段;11—新宝力格序列朱勒格单元;12—新宝力格序列花包特格单元;13—霍布序列乌兰敖包单元;14—霍布序列板申图单元;15—霍布序列那日图单元;16—花岗斑岩;17—地质界线;18—断层;19—宫忽洞铜矿床位置

Fig.1 Tectonic location (A) and regional geological map (B) of the Gonghudong copper deposit, Darhan Muminggan Joint Banner, Inner Mongolia (A−after reference [21]; B−after reference [20])

1−Quaternary; 2−Hannuoba Formation; 3−Erlian Formation; 4−Guyang Formation; 5−Suji volcanic rocks; 6−Ayadeng Formation; 7−The third member of Hujiertu Formation; 8−The second member of Hujiertu Formation; 9−The first member of Hujiertu Formation; 10−The fourth member of Baiyinbaolage Formation; 11−Zhulege unit of Xinbaolige sequence; 12−Huabaotege unit of Xinbaolige sequence; 13−Wulanaobao unit of Huobu sequence; 14−Babshentu unit of Huobu sequence; 15−Naritu unit of Huobu sequence; 16−Granite porphyry; 17−Geological boundary; 18−Fault; 19−Gonghudong copper deposit

粉砂质泥岩及藻席纹层粉晶灰岩;阿牙登组(Qn*a*)下部为浅灰色泥晶灰岩、粉砂质泥晶灰岩、白云石化泥晶灰岩夹细粒石英砂岩透镜体,上部为灰色细晶灰质白云岩、粉晶白云质灰岩,角砾状粉晶白云质灰岩夹泥质泥晶灰岩及泥质板岩[20]。苏吉火山岩(s*v*)由中性火山碎屑岩-中性熔岩-酸性火山碎屑岩-酸性熔岩组成。固阳组(K_1g)以灰绿色泥岩为主夹薄层砂岩。二连组(K_2e)为紫红色复成分砾岩、紫红色含砾泥岩夹灰绿色泥岩薄层。汉诺坝组(N_1h)为灰色块状玄武岩、气孔杏仁状玄武岩。

侵入岩在区域中部呈近东西向带状分布,主要为晚三叠世霍布序列和中侏罗世新宝力格序列花岗岩(图1-A)。晚三叠世霍布序列包括乌兰敖包单元(T_3W)、板申图单元(T_3B)和那日图单元(T_3N),岩性主要包括细粒含斑黑云母二长花岗岩、中细粒似斑状黑云母二长花岗岩、中粒二长花岗岩和中粗粒钾长花岗岩,均属二长花岗岩系列,成分变化较小但结构演化明显,由早至晚由细变粗[20]。中侏罗世新宝力格序列包括朱勒格单元(J_2Z)和花包特格单元(J_2H),其岩性主要为细粒含黑云母二长花岗岩和细粒少斑黑云母二长花岗岩。少量花岗斑岩体出露于宫忽洞铜矿床东南部。

区域主要发育中生界断裂系统,以脆性破裂为主,形成相互切割的断裂组合。断裂系统由EW向延伸北倾的逆断层组合和NW向展布的右行平移断裂组合组成,其中EW向断层被NW向断层切割错位(图1-B)。

2 矿床地质特征

宫忽洞铜矿区出露白云鄂博群白音宝拉格组四段(Qnb^4)、呼吉尔图组一段(Qnh^1)到三段(Qnh^3)、阿牙登组(Qn*a*)及二叠系下统苏吉火山岩(s*v*)(图2)。白云鄂博群白音宝拉格组四段(Qnb^4)分布于矿区南部,自下而上可划分为:①深灰色变余石英砂岩(sc^1),以石英为砂屑,绢云母、黑云母和微粒石英为胶结物;②黑云母石英板岩(sc^2),由石英、黑云母、绢云母和少量绿泥石组成;③灰白色变余石英砂岩(*dc*),以石英为砂屑,石英细粒集合体、绢云母和少量方解石为胶结物;④黑云母石英板岩(sn^1),白灰色,成分为石英、长石、少量黑云母和绢云母;⑤淡色石英岩(sn^2),灰白色,岩石成分为石英、长石、极少量黑云母和绿泥石;⑥黑云母硅质板岩(*gc*):灰色,主要为胶状或隐晶质的硅质(>80%),板理面发育少量黑云母、绢云母等新生矿物(图2)[17]。呼吉尔图组一段(Qnh^1)到三段(Qnh^3)倾向NW,倾角60°~75°,与白音宝拉格组四段(Qnb^4)呈假整合接触,总厚710 m。主要岩性有:①结晶灰岩(mg),主要为重结晶的微晶方解石(>70%),该层顶、底板中矽卡岩(*sk*)发育,铜矿体赋存于其中;②石英透辉石角岩(*zb*),主要由石英、透辉石和少量的黑云母、绢云母、绿泥石组成,下部矽卡岩化明显,局部有铜矿化;③黑云母透辉石角岩(*yb*),由黑云母、少量石英、透闪石、阳起石、绿泥石等矿物组成,该层下部局部有铜矿化形成的小矿体,自下而上角岩化逐渐变弱而过渡为石英黑云母板岩(bc^1);④石英黑云母板岩(bc^1),成分为黑云母、石英,少量绢云母;⑤黑云母板岩(bc^2),成分为黑云母、绢云母及少量石英[17]。阿牙登岩组硅质灰岩(*Ls*),呈灰色,中细粒结构,块状构造,成分主要为方解石、少量石英,厚150 m。二叠系下统苏吉火山岩(*sv*),主要岩性为凝灰岩(*dg*),是中、酸性火山碎屑沉积岩。

矿区东南小范围出露花岗斑岩,岩石呈灰白色,斑状结构,块状构造。斑晶约占30%,由石英、斜长石组成,基质为长英质显微显晶质,主要由石英和长石组成,主要矿物含量为斜长石(40%左右)、石英(35%)、钾长石(25%)等(图3)。此岩体呈岩株状侵入于白云鄂博群地层中,在与灰岩地层接触带附近具有较多的紫色萤石,在接触带上或内接触带有化探异常,并有矽卡岩存在。岩脉有闪斜煌斑岩、闪长玢岩、闪长岩、石英岩等,均呈脉状侵入于白云鄂博地层之中(图2)。

区域受南北向挤压应力作用发育3组断裂:①NEE向断层为F17,发育于结晶灰岩中;②NW—NNW向断裂最为发育,规模最大者为F10,使矿化带沿走向中断,水平断距达1200 m,小者水平断距只有2~3 m,如F20、F21,断层面一般平直,多为扭性断层,少数为压扭性断层或张扭性断层,是南北向区域挤压应力作用的结果;③NE—NNE向断层较为发育,产于矿带的NE向断层常切穿地层、矽卡岩和矿体,破坏了矿体的连续性,如F19号断层使矿体沿倾斜中断。

宫忽洞铜矿带长约1100 m,F19、F10断层将其

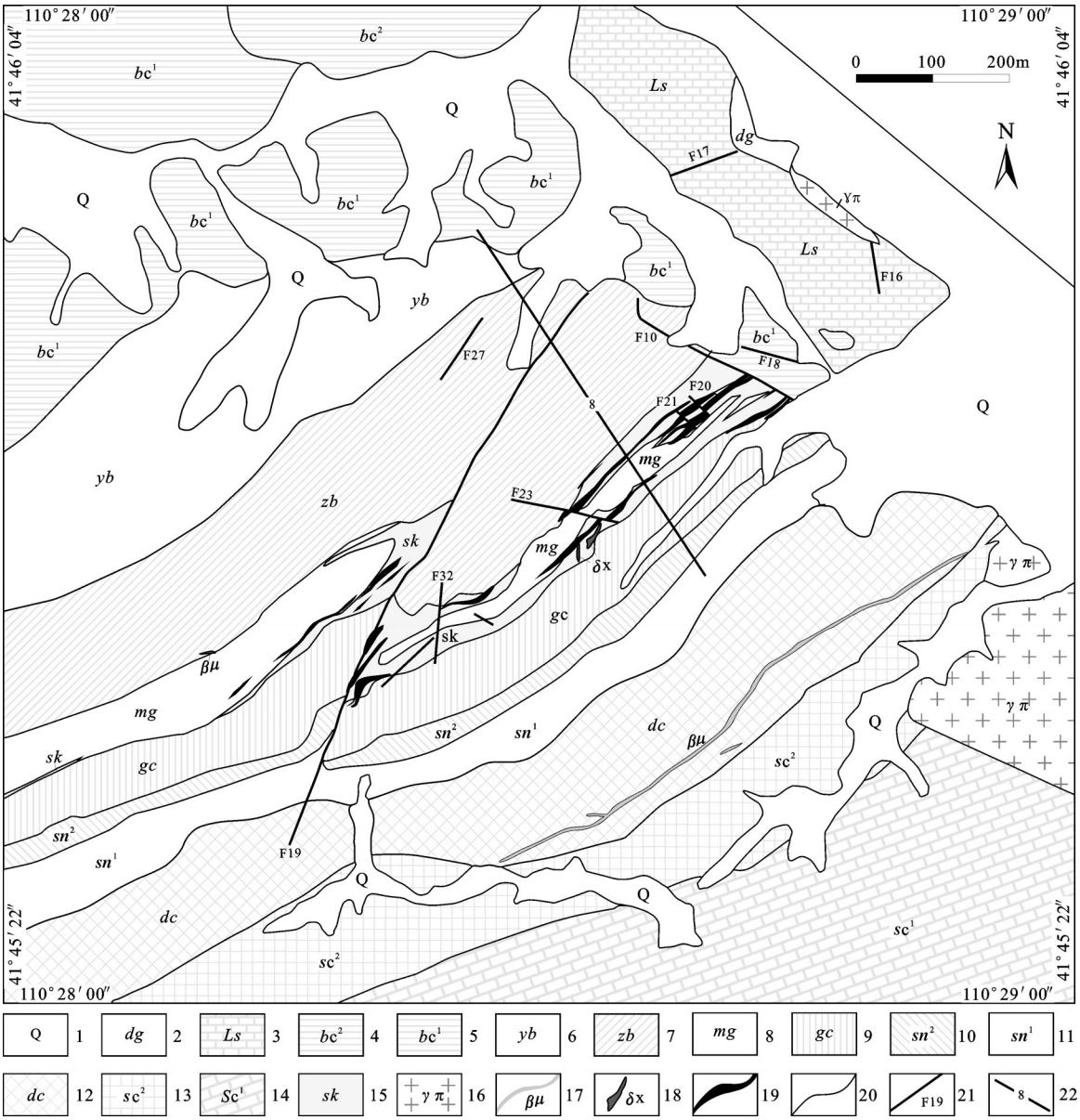

图2 内蒙古达茂旗宫忽洞铜矿床地质图(引自文献[17])

1—第四系;2—二叠系下统苏吉组凝灰岩;3—白云鄂博群阿牙登组硅质灰岩;4—白云鄂博群呼吉尔图组黑云母板岩;5—白云鄂博群呼吉尔图组石英黑云母板岩;6—白云鄂博群呼吉尔图组黑云母透闪石角岩;7—白云鄂博群呼吉尔图组石英透辉石角岩;8—白云鄂博群呼吉尔图组结晶灰岩;9—白云鄂博群白音宝拉格组黑云母硅质板岩;10—白云鄂博群白音宝拉格组淡色石英岩;11—白云鄂博群白音宝拉格组黑云母石英板岩;12—白云鄂博群白音宝拉格组黑云母变余石英砂岩;13—白云鄂博群白音宝拉格组黑云母石英板岩;14—白云鄂博群白音宝拉格组深灰色变余石英砂岩;15—矽卡岩;16—花岗斑岩;17—闪长玢岩脉;18—闪斜煌斑岩脉;19—铜矿体;20—地质界线;21—断层及编号;22—8号勘探线剖面

Fig. 2 Geological map of the Gonghudong copper deposit, Darhan Muminggan Joint Banner, Inner Mongolia (after reference [17])

1−Quaternary; 2− Tuff, Lower Permian Suji Formation; 3−Siliceous limestone, Hujiertu Formation, Bayan Obo Group; 4− Biotite slate, Hujiertu Formation, Bayan Obo Group; 5− Quartz biotite slate, Hujiertu Formation, Bayan Obo Group; 6− Biotite tremolite hornstone, Hujiertu Formation, Bayan Obo Group; 7− Biotite diopside hornstone, Hujiertu Formation, Bayan Obo Group; 8−Crystalline limestone, Hujiertu Formation, Bayan Obo Group; 9− Biotite siliceous slate, Baiyinbaolage Formation, Bayan Obo Group; 10−Tinge quartzite, Baiyinbaolage Formation, Bayan Obo Group; 11− Biotite quartz slate, Baiyinbaolage Formation, Bayan Obo Group; 12− Biotite palimpsest quartz sandstone, Baiyinbaolage Formation, Bayan Obo Group; 13− Biotite quartz slate, Baiyinbaolage Formation, Bayan Obo Group; 14−Dark gray palimpsest quartz sandstone, Baiyinbaolage Formation, Bayan Obo Group; 15−Skarn; 16− Granite porphyry; 17−Diorite−porphyrite vein; 18−Camptonite; 19−Copper orebody; 20− Geological boundary; 21−Fault; 22−No. 8 cross section

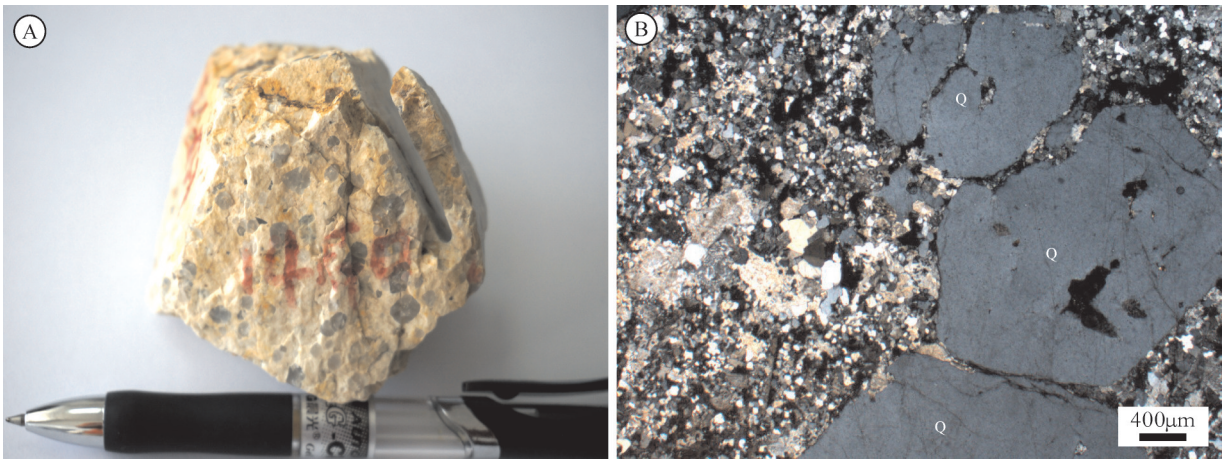

图3 宫忽洞铜矿花岗斑岩手标本(A)及显微镜下特征(正交偏光,B;Q—石英)
Fig.3 Sample (A) and microscopic (B) characteristics of granite porphyry in the Gonghudong copper deposit

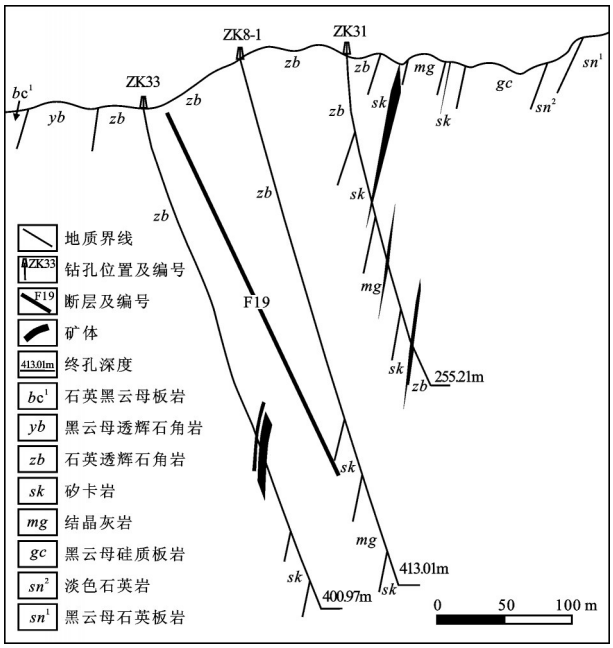

图4 内蒙古宫忽洞铜矿床8号勘探线剖面图(据文献[17]修改)
Fig.4 No. 8 cross section of the Gonghudong copper deposit, Darhan Muminggan Joint Banner, Inner Mongolia (after reference [17])

错断。共发育工业矿体16个,矿体形态可分为透镜状、似层状2种,沿走向或沿倾斜方向有分叉尖灭或膨胀收缩现象,产状与围岩基本一致(图4),走向70°~50°,倾向NW,倾角65°~80°。矿体规模大小不一,长27.23~238.66 m,厚度1.0~13.94 m,延深19.94~279.13 m。

金属矿物主要有黄铜矿、斑铜矿、闪锌矿、辉铜矿、黄铁矿、磁黄铁矿、少量磁铁矿、白铁矿、辉钼矿(图5)等。矿石发育浸染状、块状构造,少数为细脉-微细脉状构造。矿石结构包括自形晶、半自形晶以及它形粒状、结状结构(图5-a)、浸蚀结构(图5-b)、包含结构(图5-c)、交代残余结构(图5-e)、他形填隙结构(图5-d;f)等。脉石矿物有石榴石(钙铁石榴石和钙铝石榴石)、透辉石、方解石、萤石、石英、绿泥石、符山石、矽灰石、透闪石、绿帘石、蛇纹石等。

矿区东南部花岗斑岩与呼吉尔图组结晶灰岩的外接触带形成了大量矽卡岩(*sk*),主要为透辉石-石榴石矽卡岩,少数为石榴石或透辉石矽卡岩,距接触带较远的岩石则形成黑云母透闪石角岩、石英透辉石角岩等。铜的工业矿体即赋存于矽卡岩之中。围岩蚀变尚发育有硅化、萤石化、绿泥石化、绿帘石化、碳酸盐化等,其中绿泥石化及碳酸盐化与矿化关系较为密切。

3 样品及分析测试

用于锆石U-Pb定年及岩石地球化学测试的样品来自宫忽洞铜矿区东南部花岗斑岩,测试硫、铅同位素组成的样品为来自矿区采矿掌子面的新鲜矿石,测试碳、氧同位素组成的样品来自矿区的共生热液方解石脉(13GD-17,13GD-18为成矿期样

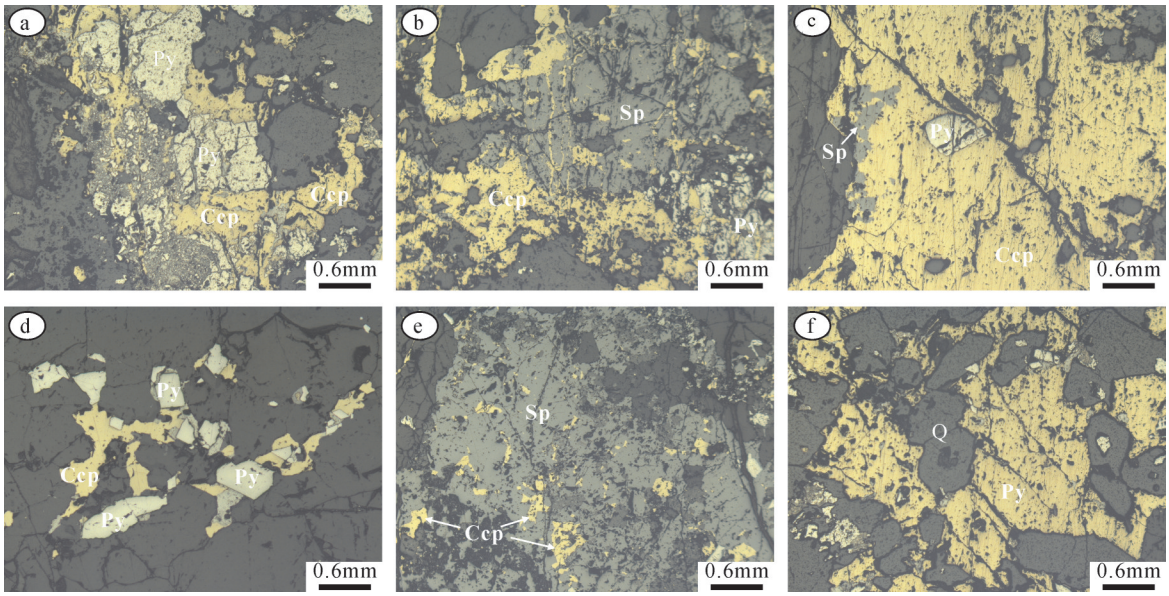

图5 宫忽洞铜矿石显微组构特征

a—黄铜矿交代黄铁矿呈结状结构;b—闪锌矿被黄铜矿浸蚀交代;c—早期半自形黄铁矿晶体被黄铜矿包含,黄铜矿边部被闪锌矿交代;d—黄铜矿呈他形晶体充填于脉石矿物或半自形黄铁矿的颗粒之间;e—黄铜矿被闪锌矿交代呈孤岛状残留结构;f—黄铜矿呈他形充填于石英等脉石矿物的粒间空隙

Sp—锌矿;Ccp—黄铜矿;Py—黄铁矿;Q—石英

Fig.5 Microscopic petrofabric characteristics of Huoshibulake Zn-Pb ore

a−Pyrite replaced by chalcopyrite exhibiting knot texture; b−Sphalerite etching replaced by chalcopyrite; c−Early stage subhedral pyrite wrapped by chalcopyrite and the edge of chalcopyrite replaced by sphalerite; d−Xenomorphic chalcopyrite filling the intergranular space of gangue minerals and subhedral pyrites; e−Chalcopyrite exhibiting island form and replaced by sphalerite; f−Xenomorphic chalcopyrite filling the intergranular space of quartz;

Sp−Sphalerite; Ccp−Chalcopyrite; Py−Pyrite; Q−Quartz

品,13GD−19为成矿晚期样品)。所有样品都挑选的是无蚀变或蚀变甚弱的样品。所有单矿物颗粒(锆石、方解石、硫化物)均由廊坊市宇能岩石矿物分选技术服务有限公司进行挑选。

挑选锆石时,首先将13GD28号样品破碎为颗粒样品,经淘洗、重磁分选,最后在双目镜下获得较多的锆石颗粒。挑选代表性锆石,黏在双面胶上,然后用无色透明的环氧树脂固定,待树脂充分固化,打磨抛光至锆石充分暴露,从而进行透、反射和CL照相,最后确定测点位置。锆石制靶在北京锆年领航科技有限公司完成,透、反射、CL照相在天津地质矿产研究所实验室完成。

锆石U−Pb定年和主量元素、微量元素分析同样在天津地质矿产研究所完成。锆石U−Pb定年采用New wave UP 193 nm激光器对锆石进行剥蚀,由Thermo Fisher公司制造的Neptune多接收电感耦合等离子体质谱仪进行测试。测试时激光束斑直径为35 μm,剥蚀深度为20~40 μm,能量密度为13~14 J/cm^2,频率为8 Hz。以GJ−1作为外部锆石年龄标样,利用NIST SRM610作为外标计算锆石的Pb、U、Th含量,采用^{208}Pb校正法对普通铅进行校正。年龄数据处理采用ICPMSDataCal程序[22],锆石加权平均年龄计算及谐和图的绘制采用Isoplot[23]进行。实验分析结果见表1,测试数据的误差均为1σ。主量元素用PW4400/40 X射线荧光光谱法进行分析测试,FeO采用氢氟酸−硫酸溶样、重铬酸钾滴定的容量法,分析精度优于2%,微量元素测试时使用X Series Ⅱ等离子体质谱仪测试,当元素含量大于10×10^{-6}时,测试精度优于5%,当元素含量<10×10^{-6}时,其精度优于10%。分析结果见表2。

硫、铅、碳、氧同位素组成的分析测试工作在核工业北京地质研究院分析测试中心进行。C、O同位素组成运用MAT 253质谱仪测定CO_2气体来获得,首先将方解石与100%的磷酸在恒温条件下反

表1 宫忽洞铜矿花岗斑岩La-MC-ICP-MS锆石U-Pb分析结果

Table 1 La-MC-ICP-MS zircon U-Pb analytical data of granite porphyry in the Gonghudong copper deposit

测点号	含量 / 10^{-6}		同位素比值								表面年龄/Ma					
	Pb	U	$^{207}Pb/^{206}Pb$	1σ	$^{207}Pb/^{235}U$	1σ	$^{206}Pb/^{238}U$	1σ	$^{232}Th/^{238}U$	1σ	$^{207}Pb/^{206}Pb$	1σ	$^{207}Pb/^{235}U$	1σ	$^{206}Pb/^{238}U$	1σ
1	22	318	0.0985	0.0015	0.6470	0.0118	0.0476	0.0003	0.8194	0.0035	1596	29	507	9	300	2
2	97	1879	0.0523	0.0008	0.3330	0.0056	0.0462	0.0003	0.5249	0.0005	298	37	292	5	291	2
3	71	1303	0.1076	0.0017	0.7068	0.0125	0.0476	0.0003	0.4782	0.0038	1759	29	543	10	300	2
4	104	1931	0.1056	0.0031	0.6938	0.0233	0.0477	0.0003	0.4657	0.0008	1724	54	535	18	300	2
5	26	374	0.1277	0.0061	0.8412	0.0654	0.0478	0.0011	0.5605	0.0109	2067	85	620	48	301	7
6	79	1489	0.1056	0.0012	0.6937	0.0082	0.0476	0.0003	0.4468	0.0010	1725	21	535	6	300	2
7	20	324	0.1002	0.0031	0.6570	0.0264	0.0476	0.0005	0.4280	0.0007	1628	57	513	21	300	3
8	14	221	0.0744	0.0017	0.4908	0.0147	0.0478	0.0005	0.5525	0.0027	1052	47	405	12	301	3
9	9	131	0.0538	0.0013	0.3501	0.0108	0.0472	0.0005	0.6233	0.0006	361	56	305	9	298	3
10	91	1714	0.0959	0.0027	0.6287	0.0195	0.0475	0.0003	0.3289	0.0020	1546	52	495	15	299	2
11	88	1636	0.0992	0.0019	0.6540	0.0134	0.0478	0.0003	0.3003	0.0006	1609	36	511	10	301	2
12	99	1858	0.0500	0.0013	0.3349	0.0093	0.0486	0.0003	0.4581	0.0014	193	58	293	8	306	2
13	20	257	0.2770	0.0041	1.8116	0.0255	0.0474	0.0004	0.3655	0.0029	3346	23	1050	15	299	3
14	5	93	0.0872	0.0037	0.5742	0.0250	0.0477	0.0004	0.3955	0.0009	1365	82	461	20	301	2
15	67	1239	0.0499	0.0006	0.3331	0.0040	0.0484	0.0003	0.3864	0.0006	191	27	292	3	305	2
16	112	2207	0.0776	0.0009	0.5072	0.0061	0.0474	0.0003	0.3498	0.0019	1137	23	417	5	299	2
17	116	2248	0.0808	0.0010	0.5290	0.0066	0.0475	0.0003	0.4202	0.0007	1216	24	431	5	299	2
18	15	189	0.0518	0.0010	0.3381	0.0076	0.0474	0.0004	0.5424	0.0019	275	43	296	7	298	2
19	125	2095	0.0543	0.0011	0.3511	0.0084	0.0469	0.0004	0.3348	0.0026	382	46	306	7	296	2

表2 宫忽洞铜矿花岗斑岩主量元素(%)、微量元素(10^{-6})分析结果

Table 2 Major (%) and trace (10^{-6}) element values of granite porphyry in the Gonghudong copper deposit

分析项目	13GD-22	13GD-23	13GD-24	13GD-25	13GD-26
SiO_2	76.69	76.66	76.22	77.17	76.71
Al_2O_3	12.11	12.32	12.31	12.13	12.27
Fe_2O_3	0.030	0.090	0.060	0.020	0.080
FeO	1.20	0.90	1.00	0.85	1.03
CaO	0.53	0.42	0.58	0.47	0.66
MgO	0.10	0.093	0.10	0.088	0.094
K_2O	4.51	4.49	4.92	4.49	4.80
Na_2O	3.64	3.94	3.77	3.82	3.66
TiO_2	0.067	0.066	0.074	0.068	0.068
P_2O_5	0.013	0.017	0.012	0.016	0.015
MnO	0.051	0.056	0.051	0.045	0.056
LOI	0.52	0.33	0.38	0.34	0.081
Total	99.46	99.38	99.48	99.51	99.52
A/CNK	1.02	1.02	0.98	1.01	0.99
A/NK	1.11	1.09	1.07	1.09	1.09
K_2O+Na_2O	8.15	8.43	8.69	8.31	8.46
K_2O/Na_2O	1.24	1.14	1.31	1.18	1.31
σ	1.97	2.11	2.27	2.02	2.12
FeO^T/MgO	12.27	10.55	10.54	9.86	11.72
La	16.7	19.7	21.0	14.1	17.7
Ce	36.7	42.8	48.2	39.7	40.5
Pr	5.13	6.90	7.14	5.08	6.17
Nd	20.1	26.0	32.2	20.3	24.8
Sm	5.52	6.83	9.80	6.53	7.98
Eu	0.031	0.053	0.055	0.046	0.030
Gd	4.65	5.44	8.70	6.49	6.65
Tb	1.01	1.04	1.73	1.44	1.61
Dy	6.82	6.60	11.2	9.80	11.1
Ho	1.46	1.37	2.15	2.05	2.36
Er	4.49	4.07	6.04	6.00	7.01
Tm	0.79	0.73	0.92	1.02	1.24
Yb	5.70	5.36	6.52	7.07	9.05
Lu	0.88	0.82	1.00	1.10	1.38
Y	38.1	31.9	57.0	52.0	64.2
ΣREE	109.98	127.71	156.66	120.73	137.58
LREE	84.18	102.28	118.40	85.76	97.18
HREE	25.80	25.43	38.26	34.97	40.40
LREE/HREE	3.26	4.02	3.09	2.45	2.41
La_N/Yb_N	2.10	2.64	2.31	1.43	1.40
δ Eu	0.02	0.03	0.02	0.02	0.01
δ Ce	0.96	0.90	0.96	1.15	0.95
Cu	6.84	18.6	7.2	8.51	10
Pb	37.6	44.5	46.4	48.6	65.4
Zn	61.6	58	51	39.9	42.4
Cr	3.79	5.9	4.28	4.7	4.46
Ni	2.45	2.64	3.18	4.25	2.95
Co	0.6	0.65	0.75	0.71	0.65
Li	55.3	6.4	7.06	11.6	13.3
Rb	314	230	243	269	258
Cs	14.7	4.03	4.19	7.63	7.49
Sr	11.4	24.5	24.9	25	16.5
Ba	21.3	60.5	61.2	54.9	44.5
V	4.03	7.01	4.71	3.94	2.49
Sc	17.8	19.2	19.1	17.5	17.5
Nb	60.2	50.5	56	51.8	55.9
Ta	5.09	6.54	5.09	5.07	5.85
Zr	110	116	113	99.3	108
Hf	7.24	7.88	7.58	6.98	7.38
Be	4.76	10.2	6.9	7.93	8.57
Ga	22.1	22.4	19.8	21.3	22.7
Ge	0.9	0.92	0.94	0.84	0.93
U	1.82	5.79	2.44	2.43	2.35
Th	29.8	31.8	37.5	31.2	32.5
F	1950	510	1680	1060	2130

应产生H_2O和CO_2气体,然后用冷冻法分离生成的水,即可收集纯净的CO_2气体,分析结果以V-PDB进行表达,计算方解石的$\delta^{18}O_{SMOW}$时,采用$\delta^{18}O_{SMOW}=1.03086\times\delta^{18}O_{PDB}+30.86$[24],分析结果见表3。硫同位素组成通过Delta v plus质谱仪测定SO_2获得,首先将硫化物单矿物与氧化亚铜按一定比例研磨,然后在高温真空条件下将S全部氧化成SO_2,用冷冻法收集后即可测试,以V-CDT为标准,$\delta^{34}S$误差为+0.2‰,分析结果见表4。铅同位素组成分析时,运用ISOPROBE-T进行测量,首先将样品用混合酸($HF+HClO_4$)进行分解,然后用树脂交换法进行铅的分离,蒸干后用热表面电离质谱法测试。测量精度对1 μg铅其$^{206}Pb/^{204}Pb$低于0.05%,$^{208}Pb/^{206}Pb$一般不大于0.005%,分析结果见表5。铅同位素H-H单阶段演化模式计算运用Faure [25]给出的公式进行,分析及计算结果见表6。

4　测试结果

4.1　锆石U-Pb年龄

宫忽洞铜矿东南部花岗斑岩(样品13GD28)锆石CL图像及分析点位见图6-c。CL图像显示,该样品锆石晶体形态相对较好,多数可见清晰的生长韵律(震荡环带),显示出岩浆锆石特征。锆石颗粒长50~180 μm,宽30~50 μm,长宽比大多在3∶1~2∶1,少数为1∶1,常见有包裹体和裂隙。对其中19个锆石颗粒进行了U-Pb同位素分析(表3),其$^{232}Th/^{238}U$比值在0.30~0.82,亦表明其为典型的岩浆锆石。锆石19个分析点有6个落在谐和线上或其附近(图6-b),其余数据点分布距谐和线较远。6个分析点$^{206}Pb/^{238}U$加权平均年龄为(299±7)Ma(n=6,MSWD=9.7,95%置信度)(图6-b),13个分析点数据在谐和线右侧近乎水平展布(图6-a),这主要与

表3 宫忽洞铜矿热液方解石碳、氧同位素分析结果(‰)
Table 3 C and O isotopic compositions of the hydrothermal calcite in the Gonghudong copper deposit(‰)

样号	矿物	$\delta^{13}C_{V-PDB}$	$\delta^{18}O_{V-PDB}$	$\delta^{18}O_{V-SMOW}$
13GD-17	成矿期方解石	-9.9	-24.3	5.9
13GD-18	成矿期方解石	-10.6	-25.5	4.6
13GD-19	成矿后期方解石	-8.6	-15.4	15

表4 宫忽洞铜矿硫化物硫同位素分析结果(‰)
Table 4 Sulfur isotopic compositions of sulfides in the Gonghudong copper deposit(‰)

样号	矿物	矿物组合	$\delta^{34}S_{V-CDT}$
13GD-10	黄铁矿	黄铁矿+黄铜矿	9.2
13GD-10	黄铜矿	黄铁矿+黄铜矿	9
13GD-7	辉钼矿	辉钼矿+磁黄铁矿+萤石	10
13GD-7	磁黄铁矿	辉钼矿+磁黄铁矿+萤石	1.2

表5 宫忽洞铜矿硫化物铅同位素组成
Table 5 Lead isotopic compositions of sulfides in the Gonghudong copper deposit

样号	矿物	$^{208}Pb/^{204}Pb$	Std err	$^{207}Pb/^{204}Pb$	Std err	$^{206}Pb/^{204}Pb$	Std err
13GD-10	黄铁矿	37.841	0.003	15.506	0.001	17.737	0.001
13GD-10	黄铜矿	37.969	0.008	15.549	0.003	17.729	0.002
13GD-7	辉钼矿	37.851	0.007	15.514	0.002	17.706	0.002
13GD-7	磁黄铁矿	37.967	0.005	15.564	0.002	17.828	0.002

表6 宫忽洞铜矿硫化物铅同位素特征参数
Table 6 Characteristic parameters of lead isotopic compositions of sulfides in the Gonghudong

样号	$^{206}Pb/^{207}Pb$	t/Ma	μ	ω	Th/U	V1	V2	△α	△β	△γ
13GD-10	1.1439	541	9.36	36.92	3.82	58.14	44.72	63.83	13.87	33.44
13GD-10	1.1402	596	9.45	37.95	3.89	65.37	46.86	68.00	17.04	39.44
13GD-7	1.1413	572	9.38	37.22	3.84	60.01	44.93	64.61	14.59	35.13
13GD-7	1.1455	543	9.46	37.49	3.84	63.79	49.32	69.45	17.67	36.97

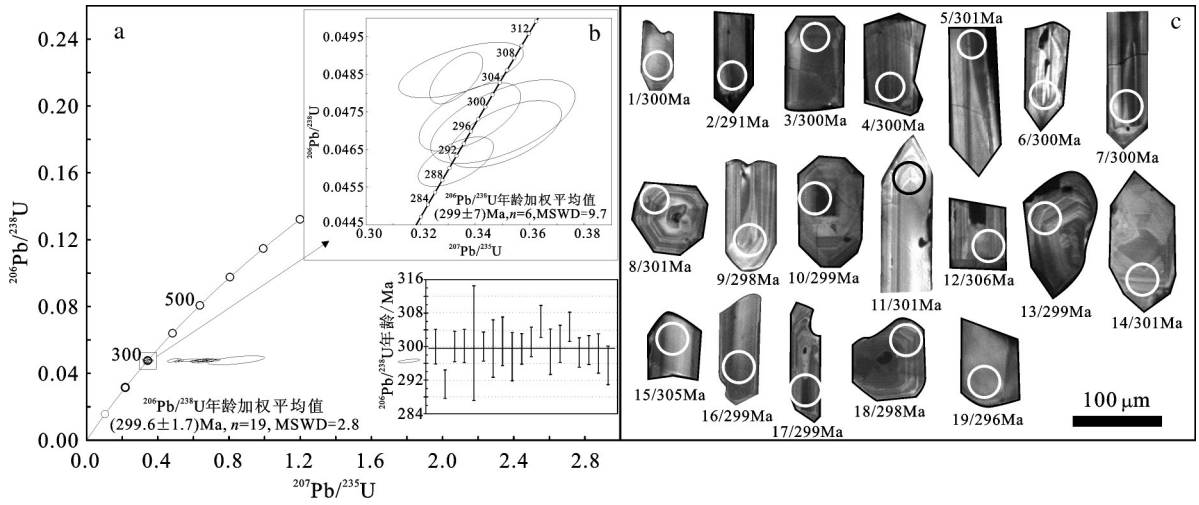

图6 宫忽洞铜矿东南部花岗斑岩锆石U−Pb年龄(a、b)和CL图像及测点号(c)

Fig.6 CL images, analytical spots (c) and U−Pb ages (a, b) of the analyzed zircon for granite porphyry in the Gonghudong copper deposit

^{207}Pb信号强度偏低使仪器测试误差较大有关,这使得$^{207}Pb/^{235}Pb$表面年龄偏高,但不影响$^{206}Pb/^{238}U$比值和表面年龄,与发生过铅丢失的分布形式有所不同[26−27]。所有样品$^{206}Pb/^{238}U$加权平均年龄为(299.6±1.7)Ma(MSWD=2.8),代表了花岗斑岩的形成时代。

4.2 岩石地球化学特征

宫忽洞铜矿床南部花岗斑岩全岩的主量、微量元素分析结果见表2。花岗斑岩具有高硅(SiO_2=76.22%~77.17%)含量,中等的铝含量(Al_2O_3=12.11%~12.32%),较高的碱含量(K_2O+Na_2O=8.13%~8.86%,平均为8.41),低P_2O_5(0.012%~0.017%)和CaO(0.42%~0.66%)含量,富钾质(K_2O/Na_2O= 1.23~1.25)。里特曼指数介于1.97~2.27;FeO^T/MgO值介于9.86~12.27,平均值为10.08。在$SiO_2-(K_2O+Na_2O)$图上,数据点全部落入花岗岩区域内(图7);在SiO_2-K_2O图上,数据点落入高钾钙碱性系列区域内(图8−a);Al_2O_3含量介于12.11%~12.32%,铝饱和指数(A/CNK)为0.98~1.02,在A/NK−A/CNK图解中位于弱准铝质与弱过铝质区域(图8−b)。

宫忽洞铜矿花岗斑岩的稀土元素球粒陨石标准化曲线较为平坦(图9−a),具有极强的负Eu异常(δEu=0.01~0.03)。稀土总量较低并且变化范围相对较小(ΣREE=109.98×10^{-6}~156.66×10^{-6},平均为130.53×10^{-6}),LREE/HREE=2.41~4.02,$(La/Yb)_N$=1.40~2.64,轻重稀土之间有一定的分馏,具有富集轻稀土元素的特点。球粒陨石标准化稀土配分曲线呈典型的"V"字形,与典型A型花岗岩稀土元素特征[28]相类似。微量元素原始地幔标准化蛛网图(图9−b)显示,宫忽洞铜矿花岗斑岩富集Rb、Th、U等大离子亲石元素(LILE)和Nd、Hf、Y等高场强元素(HFSE),明显亏损Ba、Sr、P、Ti等元素。宫忽洞

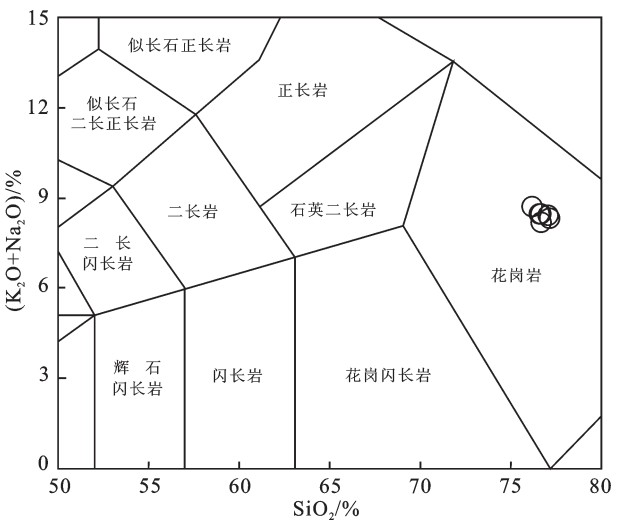

图7 内蒙古达茂旗宫忽洞铜矿床花岗斑岩的$SiO_2-(K_2O+Na_2O)$图解(底图据文献[29])

Fig.7 Granite porphyry samples from the Gonghudong copper deposit plotted on $SiO_2-(K_2O+Na_2O)$ (after reference [29])

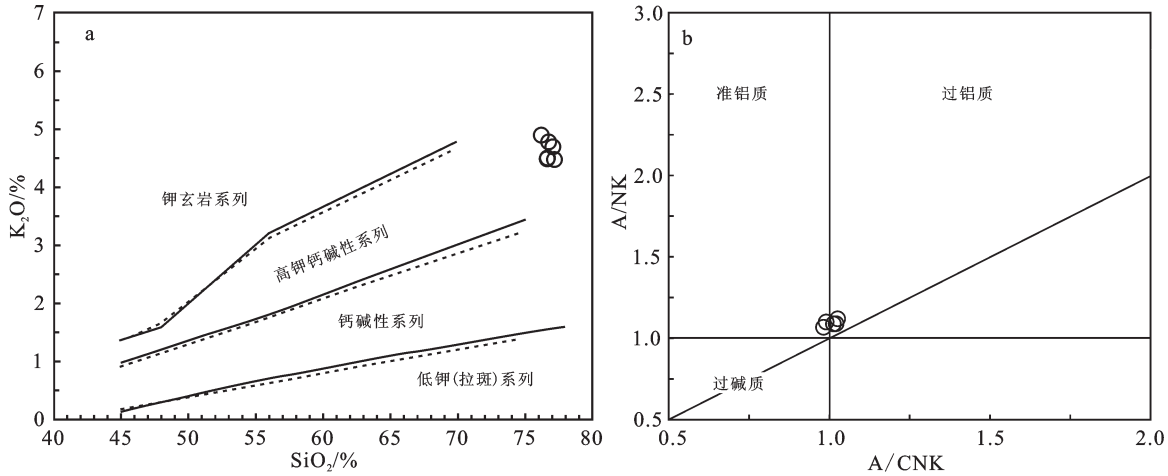

图8 宫忽洞铜矿床花岗斑岩的SiO_2−K_2O图(a,实线据文献[30]; 虚线据文献[31])和含铝指数图(b,据文献[32])

Fig. 8 SiO_2 versus K_2O diagram (a, solid line after reference [30]; dotted line after reference [31]) and aluminous index diagrams (b, after reference [32]) for granite porphyry in the Gonghudong copper deposit

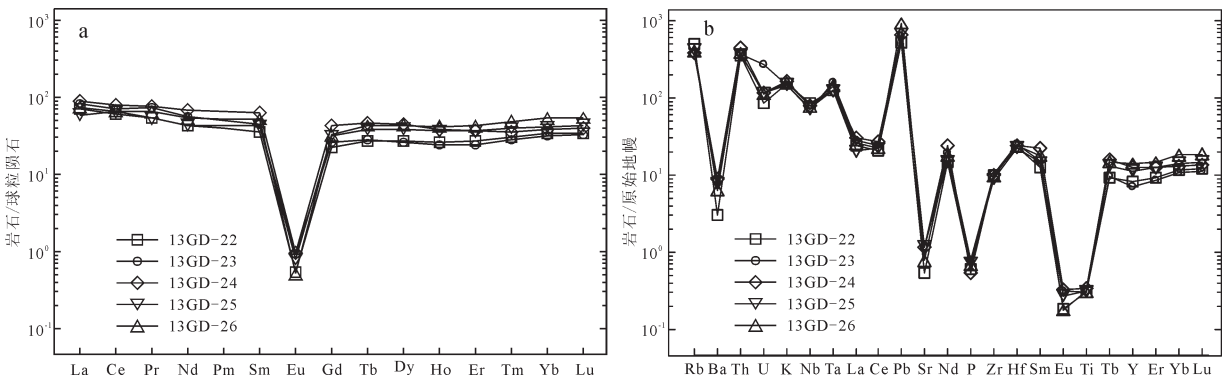

图9 宫忽洞铜矿床花岗斑岩稀土元素球粒陨石标准化配分曲线(a)和微量元素原始地幔标准化蛛网图(b)(标准化数值据文献[33])

Fig.9 Chondrite−normalized REE patterns (a) and primitive mantle−normalized trace element patterns (b) for granite porphyry in the Gonghudong copper deposit (normalized data after reference [33])

铜矿南部花岗斑岩的10000Ga/Al值变化于2.32~3.49,平均值为3.11,高于世界I型(2.25)和S型(2.39)花岗岩平均值[28],而具有A型花岗岩特征。

4.3 硫、铅、碳、氧同位素地球化学

宫忽洞铜矿床2件成矿期方解石$\delta^{13}C_{V-PDB}$值分别为−10.6‰和−9.9‰,对应的$\delta^{18}O_{V-SMOW}$值为4.6‰和5.9‰;1件成矿晚期方解石的$\delta^{13}C_{V-PDB}$值为−8.6‰,对应的$\delta^{18}O_{V-SMOW}$值为15‰(表3),可见从成矿期到成矿晚期$\delta^{13}C_{V-PDB}$值和$\delta^{18}O_{V-SMOW}$值均有增高的趋势。来自2个样品的4件不同类型硫化物的$\delta^{34}S$值介于1.2‰~10‰,平均为7.35‰,极差为8.8‰,其中3件硫化物(黄铁矿、黄铜矿、辉钼矿)样品$\delta^{34}S$值较为集中,变化于9‰~10‰;1件磁黄铁矿样品$\delta^{34}S$值为1.2‰(表4)。4件不同硫化物的$^{206}Pb/^{204}Pb$比值为17.706~17.828,均值为17.75,极差为0.122;$^{207}Pb/^{204}Pb$比值介于15.506~15.564,平均值为15.533,极差为0.058;$^{208}Pb/^{204}Pb$变化于37.841~37.969,平均值为37.907,极差为0.128,不同矿物之间的铅同位素组成不仅变化范围小且十分均一(表5)。H−H单阶段铅演化模式计算得出矿石铅的模式年龄变化于541~596 Ma,μ=9.36~9.46,平均9.41;ω=36.92~37.95,平均37.41,Th/U=3.82~3.89,平均值为3.85(表6),具有较低的Th/U值,μ值、ω值均高于正常铅范围(μ=8.99±0.07;ω=35.55±0.59;Th/U=3.92±0.09,

转引自[34])。

5 讨 论

5.1 成岩成矿时代

宫忽洞铜矿床东南部花岗斑岩的锆石U-Pb定年表明:6个在谐和线上的分析点$^{206}Pb/^{238}U$加权平均年龄为(299±7)Ma(n=6,MSWD=9.7,95%置信度)(图6-b),所有样品$^{206}Pb/^{238}U$加权平均年龄为(299.6±1.7)Ma(MSWD=2.8)(图6-a),该岩体形成于晚石炭世—早二叠世时期。此年龄与蒙古国欧玉陶勒盖铜(金)矿床正长岩体中黑云母K-Ar年龄(307±4)Ma[35]、查干苏布尔加含矿二长岩中的黑云母K-Ar年龄(313±2.9)Ma[36]等在误差范围内一致。宫忽洞铜矿是一例典型的矽卡岩型铜矿床,在其东南部花岗斑岩与呼吉尔图组结晶灰岩的内、外接触带发育有大量矽卡岩,显示成岩与成矿具有明显的时空相关关系。结合其成岩时代可以大致确定宫忽洞铜矿床是晚古生代构造岩浆活动的产物。

5.2 岩石成因类型

花岗岩通常被分为I型、S型、M型和A型4类。前3类主要由其源岩性质划分,而A型花岗岩以三“A”为特征,即碱性(Alkaline)、无水(Anhydrous)、非造山(Anorogenic),不涉及其成岩物质来源[37]。其特征为富SiO_2、高Ga、Zr、Nb和Y,贫Al_2O_3、Sr、Ba、Ti和P,REE具有明显的负Eu异常。宫忽洞铜矿南部花岗斑岩具有高Si、贫Al特征;明显亏损Ba、Sr、P、Ti等元素;10000Ga/Al值高于世界I型(2.25)和S型(2.39)花岗岩平均值[28];稀土配分曲线呈典型的“V”字形,具有典型A型花岗岩特征[28]。其FeO^T/MgO值介于9.86~12.27,平均值为10.08,明显高于全球典型M型(2.37)、I型(2.27)和S型(2.38)花岗岩[22],同样具有A型花岗岩的特征,花岗岩的P_2O_5值介于0.012%~0.017%,远低于高分异S型花岗岩的P_2O_5平均值(0.14%[38])。在A型花岗岩微量元素判别图[28]中,宫忽洞铜矿床所有样品均落入A型花岗岩的范围内(图10)。A型花岗岩亚类判别图[39]可进一步将A型花岗岩划分为A1、A2两个亚类,在图解中宫忽洞铜矿花岗斑岩均落入A1型区域内(图11)。综上所述,宫忽洞铜矿花岗斑岩成因类型为A1亚类的A型花岗岩。

5.3 构造环境判别

花岗岩的微量元素组成明显受其成岩构造环境的制约,将宫忽洞铜矿南部花岗斑岩样品投点于Rb-(Y+Nb)、Rb-(Yb+Ta)构造环境判别图解中,所

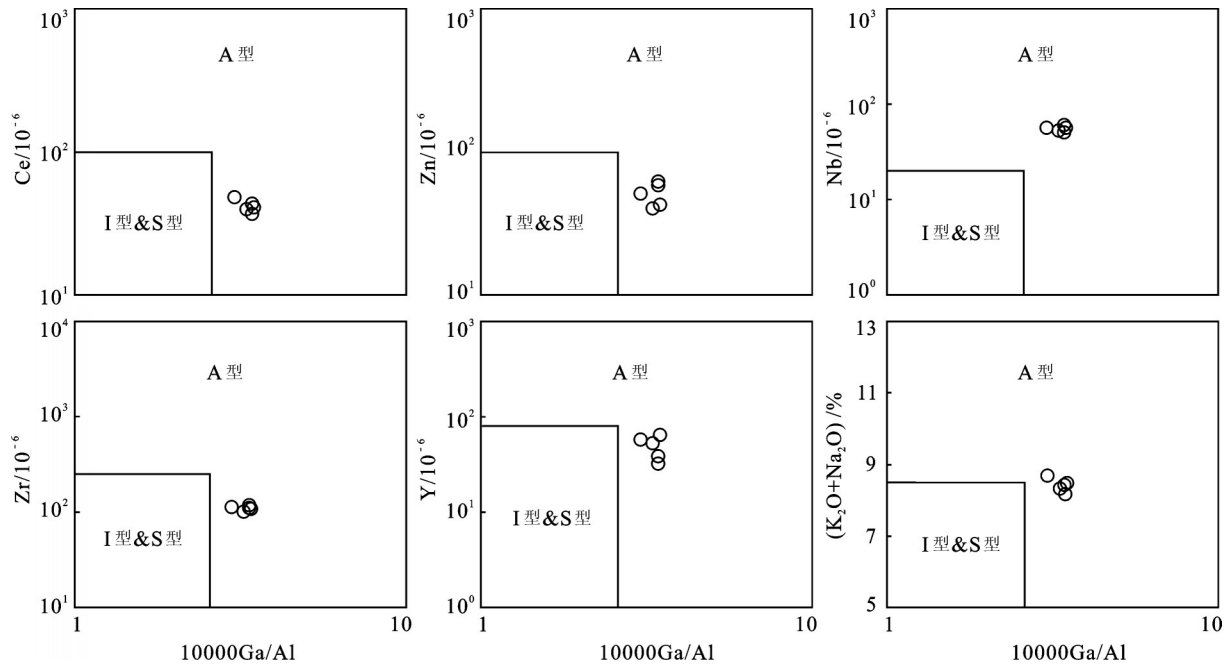

图10 宫忽洞铜矿花岗斑岩10000Ga/Al-Ce、Zn、Nb、Zr、Y和K_2O+Na_2O图解(底图据文献[28])

Fig. 10 Diagrams of 10000Ga/Al-Ce, Zn, Nb, Zr, Y and K_2O+Na_2O for granite porphyry in the Gonghudong copper deposit (after reference [28])

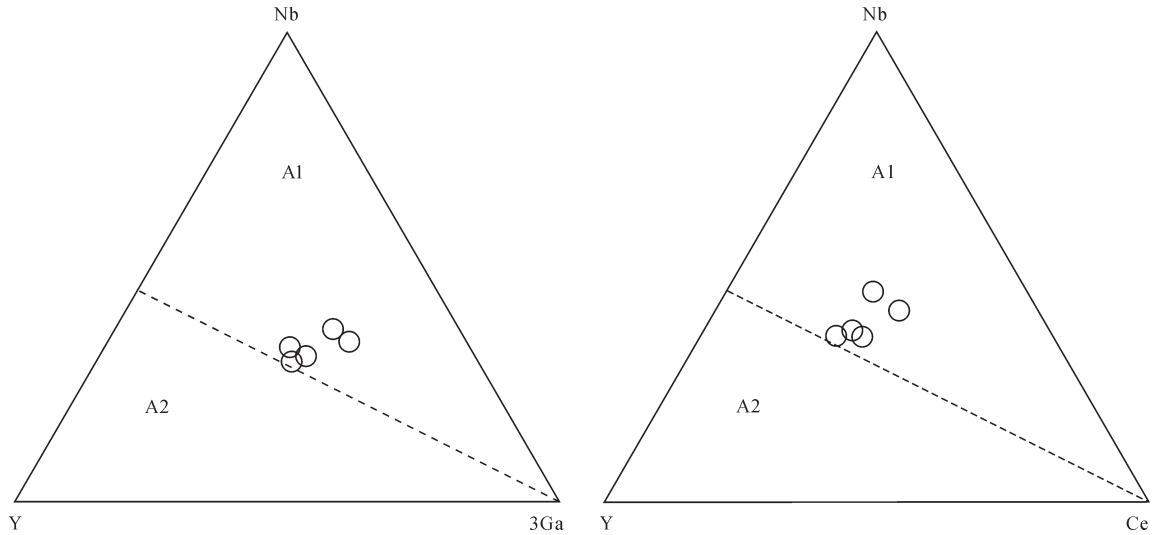

图11 宫忽洞铜矿花岗斑岩的Nb−Y−3Ga和Nb−Y−Ce图解(底图据文献[39])

Fig. 11 Nb−Y−3Ga and Nb−Y−Ce diagrams for granite porphyry in the Gonghudong copper deposit (base map after reference [39])

有样品均落入后碰撞环境及板内环境中(图12),这种环境有利于幔源岩浆底侵作用的发生,从而形成A型花岗岩[40],同样在图解中样品点具有从后碰撞环境向板内环境过渡的趋势,标志着碰撞造山阶段的结束,被称为后造山阶段[41]。在$Al_2O_3-SiO_2$、TFe/TFe+MgO−SiO_2、$R1-R2$花岗岩构造环境判别图解中(图13),样品点均落入后造山环境区域。宫忽洞铜矿东南部花岗斑岩可能是后造山拉张构造环境下的产物。

5.4 成矿物质来源

前人研究表明,成矿流体中的碳主要有3种可能来源,即:①地幔射气或岩浆结晶分异作用($\delta^{13}C_{V-}$

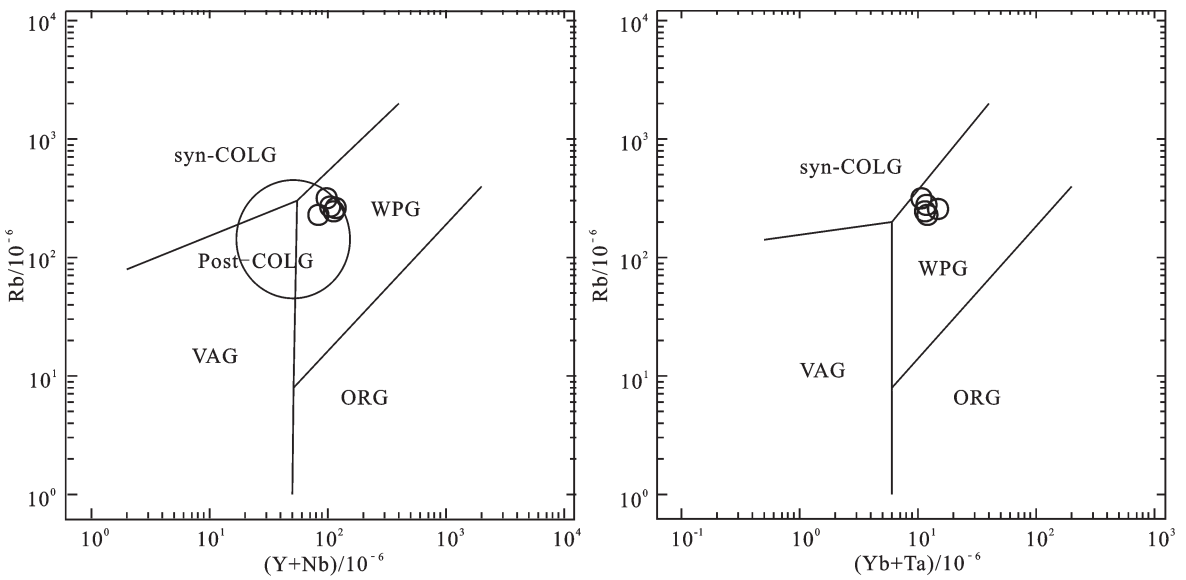

图12 宫忽洞铜矿花岗斑岩构造环境判别图解(底图据文献[42])

Syn−COLG—同碰撞花岗岩;Post−COLG—后碰撞花岗岩;VAG—火山弧花岗岩;ORG—洋脊花岗岩;WPG—板内花岗岩

Fig.12 Discrimination diagrams of tectonic setting for granite porphyry in the Gonghudong copper deposit (base map after reference [42])

Syn−COLG−Syn−collision granites; Post−COLG−Post−collision granites; VAG−Volcanic arc granites; ORG−Ocean ridge granites; WPG− Intraplate granites

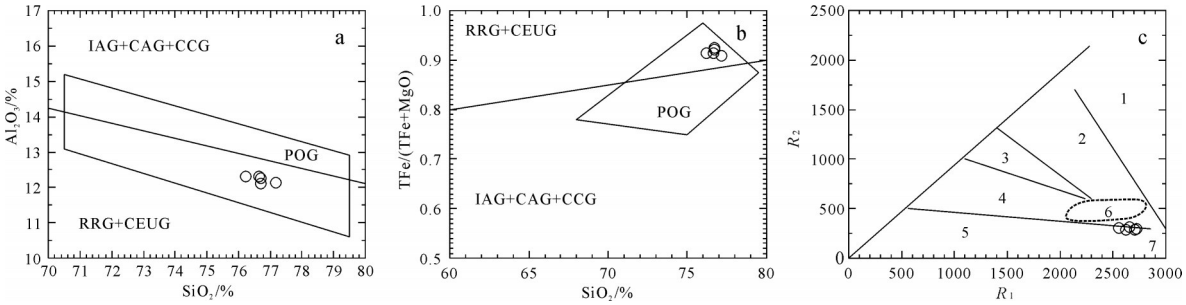

图13 宫忽洞铜矿花岗斑岩构造环境判别图解(a,b—据文献[42]; c—据文献[43])

IAG−岛弧花岗岩类;CAG−大陆弧花岗岩类;CCG−大陆碰撞花岗岩类;POG−后造山花岗岩类;RRG−与裂谷有关的花岗岩类;CEUG−与大陆陆陆抬升有关的花岗岩类;1−地幔斜长花岗岩;2−破坏性活动板块边缘(板块碰撞前)花岗岩;3−板块碰撞后隆起期花岗岩;4−晚造山期花岗岩;5−非造山区A型花岗岩;6−同碰撞(S型)花岗岩;7−造山期后A型花岗岩

Fig.13 Discrimination diagrams of tectonic setting for granite porphyry in the Gonghudong copper deposit (a,b− after reference [42]; c− after reference [43])

IAG−Island arc granite; CAG−Continent−arc granite; CCG−Continent−collision granite; POG−Post−orogenic granite; RRG−Granite related to rift; CEUG−Continent emerging−uplift granite; 1−Mantle plagioclase granite; 2−Granite before plate collision; 3−Uplifted granite after plate collision; 4−Late orogenic granite; 5−A−type granite of nonorogenic area; 6−Syn−collision granite; 7−Post−orogenic A−type granite

$_{PDB}$值变化范围分别为−5‰~−2‰、−9‰~−3‰)[44];②海相碳酸盐岩溶解和去碳酸作用,这种来源的碳同位素组成具有重碳同位素的特征,其$\delta^{13}C_{V-PDB}$值介于−2‰~3‰[45];③有机质脱羟基和氧化作用,其碳同位素组成很低,$\delta^{13}C_{V-PDB}$值介于−30‰~−15‰,平均−22‰[46],不同源区CO_2的碳、氧同位素具有不同的分馏趋势(图14)。宫忽洞铜矿床3件方解石$\delta^{13}C_{V-PDB}$值分别为−10.6、−9.9和−8.6,相对邻近岩浆结晶分异作用的范围,结合$\delta^{13}C_{V-PDB}-\delta^{18}O_{V-SMOW}$图解(图14),相对靠近结晶分异作用和沉积岩混染分布区,宫忽洞铜矿床成矿期的CO_2可能由花岗斑岩与灰岩地层的相互作用形成。

已有研究表明,地球上硫有3个储库,一是幔源硫,其$\delta^{34}S$值为−3‰~3‰;二是海水硫,其$\delta^{34}S$值为20%左右;三是沉积物中的还原硫,其硫同位素组成以具有较大的负值为主[51]。宫忽洞铜矿4件硫化物$\delta^{34}S$值介于1.2‰~10‰,平均为7.35‰,极差为8.8‰。宫忽洞铜矿硫化物极差相对较大,表明矿床可能并非单一硫源;在同一件样品中的不同硫化物间具有$\delta^{34}S_{黄铁矿}>\delta^{34}S_{黄铜矿}$、$\delta^{34}S_{辉钼矿}>\delta^{34}S_{磁黄铁矿}$的特征,

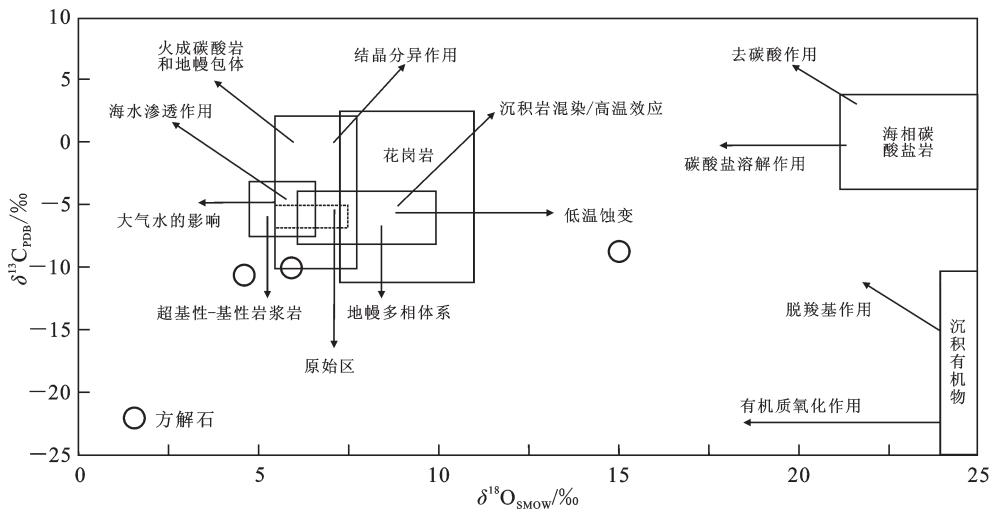

图14 宫忽洞铜矿床热液方解石的$\delta^{13}C_{V-PDB}-\delta^{18}O_{V-SMOW}$图解(底图据文献[47−50]修改)

Fig.14 The $\delta^{13}C_{V-PDB}-\delta^{18}O_{V-SMOW}$ diagram of the hydrothermal calcite in the Gonghudong copper deposit (base diagram modified after reference [47−50])

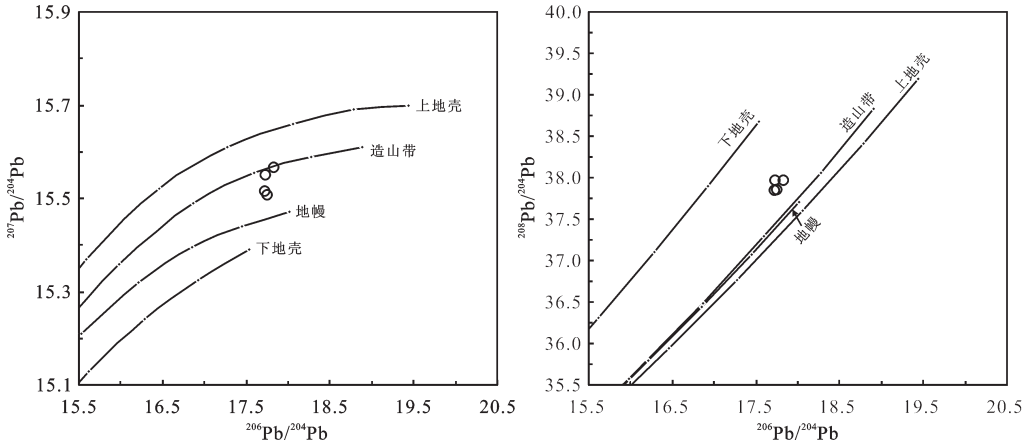

图15 宫忽洞铜矿床硫化物铅同位素构造模式图(底图据[54])

Fig. 15 Tectonic model of the $^{208}Pb/^{204}Pb$ versus $^{206}Pb/^{204}Pb$ and $^{207}Pb/^{204}Pb$ versus $^{206}Pb/^{204}Pb$ of sulfides in the Gonghudong copper deposit (after reference [54])

表明硫化物在沉淀过程中硫同位素分馏基本达到平衡。3件硫化物(黄铁矿、黄铜矿、辉钼矿)具有较高的$\delta^{34}S$值,介于9‰~10‰,暗示成矿硫可能来自于海相硫酸盐或岩浆硫与海相硫酸盐的混合;而1件磁黄铁矿样品$\delta^{34}S$值为1.2‰,明显指示岩浆硫特征。总体上,宫忽洞铜矿床成矿所需的硫可能来自于岩浆硫与海相硫酸盐的混合。

宫忽洞铜矿床铅同位素组成不仅变化范围较小且十分均一,$^{206}Pb/^{204}Pb$比值极差为0.122、$^{207}Pb/^{204}Pb$比值极差为0.058、$^{208}Pb/^{204}Pb$为比值极差为0.128,稳定的铅同位素组成表明放射性成因铅含量很低。宫忽洞铜矿具有相对较高的μ值,可能指示上地壳来源特征[52]。将所有样品投点于铅构造模式图,所有样品均靠近造山带演化线(图15),同样在$\Delta\beta-\Delta\gamma$成因分类图解[53]中,所有样品也投点于造山带铅范围或其附近(图16)。宫忽洞铜矿铅同位素组成特征指示成矿物质与古亚洲洋闭合过程中的造山运动相关,而后造山阶段拉张环境形成的A型花岗斑岩体可能是成矿物质的主要提供者。

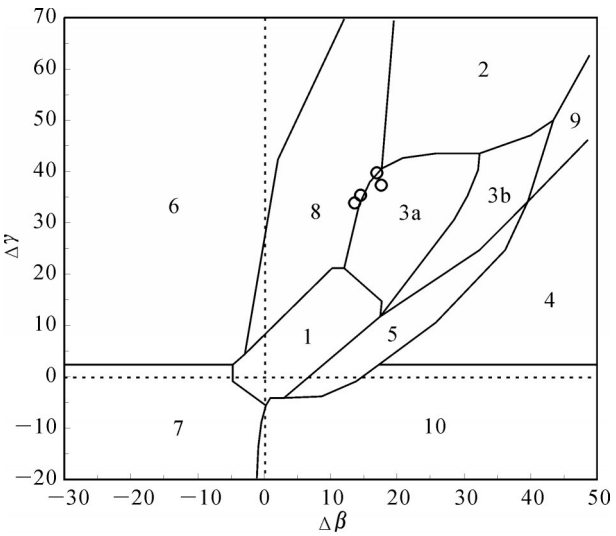

图16 宫忽洞铜矿硫化物铅同位素的$\Delta\beta-\Delta\gamma$成因分类图解(底图据[53])

1—地幔源铅;2—上地壳铅;3—上地壳与地幔混合的俯冲带铅(3a、岩浆作用;3b、沉积作用);4—化学沉积型铅;5—海底热水作用铅;6—中深变质作用铅;7—深变质下地壳铅;8—造山带铅;9—古老页岩上地壳铅;10—退变质铅;$\Delta\beta=1000\times\beta/(\beta_M-1)$,$\Delta\gamma=1000\times\gamma/(\gamma_M-1)$,$\beta$、$\gamma$和$\beta_M$、$\gamma_M$分别为样品和地幔的$^{207}Pb/^{204}Pb$和$^{208}Pb/^{204}Pb$

Fig.16 $\Delta\beta-\Delta\gamma$ genetic classification diagram of lead isotope of sulfides in the Gonghudong copper deposit (base map after [53])

1−Mantle−derived lead; 2−Upper crust lead; 3−Mixed lead of the upper crust and mantle subduction zones (3a Magmatism, 3b Sedimentation); 4−Chemical sedimentary lead; 5−Submarine hydrothermal lead; 6−Medium−high grade metamorphism lead; 7−Lower crust lead of high grade metamorphism; 8−Orogenic belt lead; 9−Upper crust lead of ancient shale; 10−Retrograde metamorphism lead; $\Delta\beta=1000\times\beta/(\beta_M-1)$, $\Delta\gamma=1000\times\gamma/(\gamma_M-1)$, β and γ are ratios of $^{207}Pb/^{204}Pb$ and $^{208}Pb/^{204}Pb$ respectively in samples, β_M and γ_M are ratios of $^{207}Pb/^{204}Pb$ and $^{208}Pb/^{204}Pb$ respectively in mantle

6 结　论

内蒙古达茂旗宫忽洞矽卡岩型铜矿床位于华北板块北缘中段中元古代白云鄂博裂谷带内,赋存于矿区东南部花岗斑岩与呼吉尔图组结晶灰岩形成的矽卡岩中。矿体呈透镜状、似层状分布,主要金属矿物为黄铜矿、斑铜矿、闪锌矿、辉铜矿、黄铁矿、磁黄铁矿等,脉石矿物为石榴石(钙铁石榴石和

钙铝石榴石)、透辉石、方解石、萤石等。矽卡岩类主要为透辉石-石榴石矽卡岩,少数为石榴石或透辉石矽卡岩。

矿区东南部花岗斑岩LA-ICP-MS锆石U-Pb定年结果为(299.6±1.7)Ma,表明该岩体形成于晚石炭世—早二叠世时期,可判定宫忽洞铜矿床是晚古生代构造岩浆活动的产物。花岗斑岩岩石地球化学特征表明其成因类型为A1亚类的A型花岗岩,可能形成于后造山拉张构造环境。C、O、S、Pb同位素研究表明,宫忽洞铜矿床成矿期的CO_2可能由花岗斑岩与灰岩地层的相互作用形成;成矿所需的硫可能来自于岩浆硫与海相硫酸盐的混合;后造山阶段拉张环境形成的A型花岗斑岩体可能是成矿物质的主要提供者。

参考文献(References):

[1]聂凤军, 江思宏, 张义, 等. 中蒙边境及邻区斑岩型铜矿床地质特征及成因[J]. 矿床地质, 2004, 23(2): 176-189.
Nie Fengjun, Jiang Sihong, Zhang Yi, et al. Geological features and origin of porphyry copper deposits in China- Mongolia border region and its neighboring areas [J]. Mineral Deposits, 2004, 23(2): 176-189(in Chinese with English abstract).

[2] 王守光, 黄占起, 苏新旭, 等. 一条值得重视的跨国境成矿带——南戈壁—东乌旗铜多金属成矿带[J]. 地学前缘, 2004, 11(1): 249-255.
Wang Shouguang, Huang Zhanqi, Su Xinxu, et al. A notable metallogenic belt striding across the border between China and Mongolia— South Gobi- Dongwuqi copper- polymetallic metallogenic belt[J]. Earth Science Frontiers, 2004, 11(1): 249-255 (in Chinese with English abstract).

[3] 余学中, 薛春纪, 丛丽娟, 等. 二连浩特一带境内外构造-成矿带的衔接问题浅析[J]. 地学前缘, 2011, 18(2): 231-241.
Yu Xuezhong, Xue Chunji, Cong Lijuan, et al. A study of the connection of faults and metallogenic belts between Erenhot Region, China and South Gobi, Mongolia[J]. Earth Science Frontiers, 2011, 18(2): 231-241(in Chinese with English abstract).

[4] 汤超, 陈军强, 刘晓雪, 等.内蒙古达茂旗北部岩浆活动与铜金成矿作用[J]. 地质与勘探, 2013, 49(2): 224-235.
Tang Chao, Chen Junqiang, Liu Xiaoxue, et al. Magmatic activities and copper and gold mineralization in northern Damaoqi, Inner Mongolia[J]. Geology and Exploration, 2013, 49(2): 224- 235(in Chinese with English abstract).

[5] 张义, 聂凤军, 江思宏, 等. 中蒙边境欧玉陶勒盖大型铜-金矿床的发现及对找矿勘查工作的启示[J]. 地质通报, 2003, 22(9): 708-712.
Zhang Yi, Nie Fengjun, Jiang Sihong, et al. Discovery of the Ouyu Tolgoi copper- gold deposit in the Sino- Mongolia border region and its significance for mineral exploration[J]. Geological Bulletin of China, 2003, 22(9): 708-712 (in Chinese with English abstract).

[6] 刘益康, 徐叶兵. 蒙古Oyu Tolgoi斑岩铜金矿的勘查[J]. 地质与勘探, 2003, 39(1):1-4.
Liu Yikang, Xu Yebing. The prospecting and main features of Oyu tolgoi porphyry Cu- Au deposit in Mongolia[J]. Geology and Exploration, 2003, 39(1):1-4(in Chinese with English abstract).

[7] 王大为, 邹治平, 李绍雄. 甘肃公婆泉铜矿成矿地质特征及矿床成因[J]. 西北地质科学, 1995, 16(1): 115-122.
Wang Dawei, Zou Zhiping, Li Shaoxiong. On the ore- forming geological features and ore deposit genesis of Gongpoquan copper deposit, Gansu Province[J]. Northwest Geoscience, 1995, 16(1): 115-122(in Chinese with English abstract).

[8] 聂凤军, 江思宏, 白大明, 等.内蒙古北山及邻区金属矿床类型及其时空分布[J]. 地质学报, 2003, 77(3): 367-378.
Nie Fengjun, Jiang Sihong, Bai Daming, et al. Type and temporal- spatial distribution of metal deposits in the Beishan mountains, Inner Mongolia, and its Neighboring region[J]. Acta Geologica Sinica, 2003, 77(3): 367-378(in Chinese with English abstract).

[9] 薛春纪, 赵战锋, 吴淦国, 等. 中亚构造域多期叠加斑岩铜矿化:以阿尔泰东南缘哈腊苏铜矿床地质、地球化学和成岩成矿时代研究为例[J]. 地学前缘, 2010, 17(2): 53-82.
Xue Chunji, Zhao Zhanfeng, Wu Gan'guo, et al. The multiperiodic superimposed porphyry copper mineralization in Central Asian Tectonic Region: A case study of geology, geochemistry and chronology of Halasu copper deposit, Southeastern Aaltai, China[J]. Earth Science Frontiers, 2010, 17(2): 53- 82 (in Chinese with English abstract).

[10] 申萍, 潘鸿迪, 董连慧, 等. 新疆延东斑岩铜矿床火山机构、容矿岩石及热液蚀变[J]. 岩石学报, 2012, 28(7): 1966-1980.
Shen Ping, Pan Hongdi, Dong Lianhui, et al. Caldera complex, hosted rocks and alteration of the Yandong porphyry copper deposit in eastern Tianshan, Xinjiang[J]. Acta Petrologica Sinica, 2012, 28(7):1966-1980(in Chinese with English abstract).

[11] 刘晓雪, 毛德宝, 曹秀兰, 等. 内蒙古查干诺尔铜矿区矿石特征及成因探讨[J]. 地质调查与研究, 2007, 30(4): 271-276.
Liu Xiaoxue, Mao Debao, Cao Xiulan, et al. Characters and Genesis of the Chaganuoer Copper Deposit in Inner Mongolia[J]. Geological Survey and Research, 2007, 30(4): 271- 276(in Chinese with English abstract).

[12] 任军平, 张连营, 唐文龙, 等.内蒙古达茂旗查干若尔铜矿区构造特征浅析[J]. 地质调查与研究, 2010, 33(2): 130-133.
Ren Junping, Zhang Lianying, Tang Wenlong, et al. Study on the structural features of the Chagannuoer copper deposit in Damaoqi, Inner Mongolia[J]. Geological Survey and Research, 2010, 33(2): 130-133(in Chinese with English abstract).

[13] 陈军强, 李志丹, 汤超, 等. 内蒙古哈布齐尔金矿床地质及物化探特征[J]. 中国矿业, 2013, 22(6): 62-65.

Chen Junqiang, Li Zhidan, Tang Chao, et al. Geophysical, geochemical and geological characteristics of Habuqier gold deposit in Inner Mongolia[J]. China Mining Magazine, 2013, 22 (6): 62−65(in Chinese with English abstract).

[14] 齐钒宇, 张志, 祝新友, 等. 湖南黄沙坪钨钼多金属矿床矽卡岩地球化学特征及其地质意义[J]. 中国地质, 2012, 39(2): 338−348.
Qi Fanyu, Zhang Zhi, Zhu Xinyou, et al. Skarn geochemistry of the Huangshaping W−Mo polymetallic deposit in Hunan and its geological significance[J]. Geology in China, 2012, 39(2): 338−348(in Chinese with English abstract).

[15] 王立强, 唐菊兴, 陈伟, 等. 西藏邦铺钼多金属矿床矽卡岩矿物学特征及其地质意义[J]. 中国地质, 2014, 41(2): 562−576.
Wang Liqiang, Tang Juxing, Chen Wei, et al. Mineralogical characteristics of skarn in the Bangpu Mo polymetallic deposit, Tibet, and their geological significance[J]. Geology in China, 2014, 41(2): 562−576(in Chinese with English abstract).

[16] 曾红, 柴凤梅, 周刚, 等. 新疆雅满苏铁矿床矽卡岩和磁铁矿矿物学特征及其地质意义[J]. 中国地质, 2014, 41(6): 1914−1928.
Zeng Hong, Chai Fengmei, Zhou Gang, et al. Mineralogy of skarn and magnetite of the Yamansu iron deposit and its geological significance[J]. Geology in China, 2014, 41(6): 1914− 1928(in Chinese with English abstract).

[17] 刘章顺, 燕振云, 巴福臣, 等. 内蒙古自治区达尔罕茂名安联合旗宫忽洞矿区铜矿详查报告[R]. 包头市同孚矿业有限公司. 2008, 1−112.
Liu Zhangshun, Yan Zhenyun, Ba Fuchen, et al. General Exploration Report of Gonghudong Copper Deposit, Darhan Muminggan Joint Banner[R]. Tongfu Mining limited company. 2008, 1−112 (in Chinese).

[18] 王楫, 李双庆, 王保良. 狼山−白云鄂博裂谷系[C]//中国北方板块构造丛书. 北京: 北京大学出版社, 1989, 1−130.
Wang Ji, Li Shuangqing, Wang Baoliang. The Langshan−Baiyunobo rift systems [C]//Contributions to the Plate Tectonics in North China. Beijing: Peking University Press, 1989, 1− 130 (in Chinese with English abstract).

[19] 聂凤军, 江思宏, 侯万荣, 等. 内蒙古中西部浅变质岩为容矿围岩的金矿床地质特征及形成过程[J]. 矿床地质, 2010, 29(1): 58−70.
Nie Fengjun, Jiang Sihong, Hou Wanrong, et al. Geological features and genesis of gold deposits hosted by low− grade metamorphic rocks in central− western Inner Mongolia [J]. Mineral Deposits, 2010, 29(1): 58− 70(in Chinese with English abstract).

[20] 李尚林,等. 达尔罕茂明安联合旗幅1∶5万区域地质调查图幅说明书[R]. 内蒙古第一区域地质研究院. 1997.
Li Shanglin, et al. Regional Geological Survey Mappable Unit Specification of Darhan Muminggan Joint Banner[R]. No. 1 Regional Geological Survey and Research Institute of Inner Mongolia. 1997.

[21] 张玉清, 张明, 贺锋, 等. 内蒙古自治区矿产资源潜力评价成果报告[R]. 内蒙古国土资源厅. 2011.
Zhang Yuqing, Zhang Ming, He Feng, et al. Mineral resource Potential Assessment Report of Inner Mongolia[R]. Office of Land and Resources of Inner Mongolia. 2011 (in Chinese).

[22] Liu Y S, Gao S, Hu Z C, et al. Continental and oceanic crust recycling− induced melt− peridotite interactions in the Trans−North China Orogen: U− Pb dating, Hf isotopes and trace elements in zircons from mantle xenoliths[J]. J. Petrol., 2010, 51 (1/2): 537−571.

[23] Ludwig K R. Users manual for isoplot/Ex (rsv.3.0): A Geochronologica Toolkit for Microsoft excel: berkrley Geochronology Center[J]. Special Publication, 2003, No.1a, 1−55.

[24] Friedman I , O'Neil J R. Compilation of stable isotope fractionation factors of geochemical interest[M]. U.S. Geological Survey, 1977, Prof. Paper 440−KK, 6th Edition.

[25] Faure G. Principles of Isotope Geology, Second edition[M]. John Wiley and Sons, New York, 1986: 1−589.

[26] Compston W, Williams I S, Kirschvink J L, et al. Zircon U−Pb ages for the Early Cambrian time− scale[J]. Journal of the Geological Society, 1992, 149(2):171−184.

[27] Zhu J C, Wang R C, Zheng P H, et al. Zircon U− Pb geochronological framework of Qitianling granite batholith, middle part of Nanling Range, South China[J]. Science in China (Series D), 2009, 52(9):1279−1294.

[28] Whalen J B, Currie K L, Chappell B W. A− type granites: Geochemical characteristics, discrimination and petrogenesis. Contributions to Mineralogy and Petrology, 1987, 95(4): 407−419.

[29] Middlemost E A K. Naming materials in the magma/igneous rock system[J]. Earth−Science Reviews, 1994, 37: 215−224.

[30] Peccerillo R, Taylor S R. Geochemistry of Eocene calc−alkaline volcanic rocks from the Kastamonu area, Northern Turkey[J]. Contributions to Mineralogy and Petrology, 1976, 58(1): 63−81.

[31] Middlemost E A K. Magmas and Magmatic Rocks[M]. London: Longman, 1985: 1−266.

[32] Maniar P D and Piccoli P M. Tectonic discrimination of granitoids[J]. Geological Society of America Bulletin, 1989, 101 (5): 635−643.

[33] Sun S S, McDonough W F. Chemical and isotopic systematics of oceanic basalts: Implications for mantle composition and processes[J]. Geological Society, Special Publications, 1989, 42: 313−345.

[34] 王立强, 顾雪祥, 程文斌, 等. 西藏蒙亚啊铅锌矿床S、Pb同位素组成及对成矿物质来源的示踪[J]. 现代地质, 2010, 24 (1): 52−58.
Wang Liqiang, Gu Xuexiang, Cheng Wenbin, et al. Sulfur and lead isotope composition and tracing for the sources of ore−forming materials in the Mengya'a Pb− Zn deposit, Tibet[J]. Geoscience, 2010, 24 (1): 52− 58(in Chinese with English

abstract).

[35] Perello J, Cox D, Garamjav D, et al. Oyu Tolgoi, Mongolia: Siluro− Devonian porphyry Cu− Au− (Mo) and high sulfidation Cu mineralization with a Cretaceous chalcocite blanket[J]. Econ. Geol., 2001, 96: 1407−1428.

[36] Lamb M A, Badarch G. Paleozoic sedimentary basins and volcanic− arc systems of southern Mongolia: New stratigraphic and sedimentologic constraints[J]. International Geology Reviews, 1997, 39, 542−576.

[37] Loiselle M C, Wones D R. Characteristics and origin of anorogenic granites[J]. Geological Society of America (Abstracts with Programs), 1979, 11:468.

[38] King P L, White A J R, Chappell B W, et al. Characterization and origin of aluminous A−type granites from the Lachlan Fold Belt, Southeastern Australia[J]. Journal of Petrology, 1997, 38: 371−391.

[39] Eby G N. The A type granitoids: A review of their occurrence and chemical characteristics and speculations on their petrogenesis[J]. Lithos, 1990, 26(1/2):115−134.

[40] 肖庆辉, 王涛, 邓晋福, 等. 中国典型造山带花岗岩与大陆地壳生长研究[M]. 北京: 地质出版社, 2009: 1−107.
Xiao Qinghui, Wang Tao, Deng Jinfu, et al. Research on China Typical Orogenic Granitoids and Continental Crustal Growth[M]. Beijing: Geological Publishing House, 2009: 1−107(in Chinese).

[41] 肖庆辉, 邓晋福, 马大铨, 等. 花岗岩研究思维与方法[M]. 北京: 地质出版社, 2002: 1−294.
Xiao Qinghui, Deng Jinfu, Ma Daquan, et al. The Ways of Investigation on Granitoids [M]. Beijing: Geological Publishing House, 2002: 1−294(in Chinese).

[42] Pearce J A. Source and settings of granitic rocks[J]. Episodes, 1996, 19: 120−125.

[43] Batchelor R A, Bowden P. Petrogenetic interpretation of granitoid rock series using multicationic parameters[J]. Chemical Geology, 1985, 48(1−4): 43−55.

[44] Taylor B E. Magmatic volatiles: Isotope variation of C, H and S reviews in mineralogy[J]. Reviews in Mineralogy and Geochemistry, 1986, 16(1): 185−255.

[45] Veizer J, Holser W T, Wilgus C K. Correlation of $^{13}C/^{12}C$ and $^{34}S/^{32}S$ secular variation[J]. Geochim. Cosmochim. Acta, 1980, 44: 579−588.

[46] Ohmoto H. Systematics of sulfer and carbon isotopes in hydrothermal ore deposits[J]. Econ. Geol., 1972, 67(5): 551−578.

[47] 刘建明, 刘家军, 顾雪祥. 沉积盆地中的流体活动及其成矿作用[J]. 岩石矿物学杂志, 1997, 16(4): 341−352.
Liu Jianmin, Liu Jiajun, Gu Xuexiang. Basin fluids and their related ore deposits[J]. Acta Petrologica et Mineralogical, 1997, 16 (4): 341−352(in Chinese with English abstract).

[48] 毛景文, 赫英, 丁悌平. 胶东金矿形成期间地幔流体参与成矿过程的碳氢氧同位素证据[J]. 矿床地质, 2002, 21(2): 121−128.
Mao Jingwen, He Ying, Ding Tiping. Mantle fluids involved in metallogenesis of Jiaodong (East Shandong) Gold district: evidence of C, O and H isotopes[J]. Mineral Deposits, 2002, 21 (2): 121−128(in Chinese with English abstract).

[49] 刘家军, 何明勤, 李志明, 等. 云南白秧坪银铜多金属矿集区碳氧同位素组成及其意义[J]. 矿床地质, 2004, 23(1): 1−10.
Liu Jiajun, He Mingqin, Li Zhimin, et al. Oxygen and carbon isotopic geochemistry of Baiyangping silver−copper polymetallic ore concentration area in Lanping basin of Yunnan Province and its significance[J]. Mineral Deposits, 2004, 23(1): 1− 10(in Chinese with English abstract).

[50] Keller J, Hoefs J. Stable Isotope Characteristics of Recent Natrocarbonatites from Oldoinyo Lengai[C]//Bell K, Keller J (ed.). Carbonatite Volcanism: Oldoinyo Lengai and the Petrogenesis of Natrocarbonatites[M]. Berlin: Springer, 1995: 113−123.

[51] Chaussidon M, Albarède F, Sheppard S M F. Sulfur isotope variations in the mantle from ion microprobe analyses of micro−sulphide inclusions[J]. Earth and Planetary Science Letters, 1989, 92: 144−156.

[52] 吴开兴, 胡瑞忠, 毕献武, 等. 矿石铅同位素示踪成矿物质来源综述[J]. 地质地球化学, 2002, 30(3): 73−81.
Wu Kaixing, Hu Ruizhong, Bi Xianwu, et al. Ore lead isotopes as a tracer for ore−forming material sources: a review[J]. Geology−Geochemistry, 2002, 30(3): 73− 81 (in Chinese with English abstract).

[53] 朱炳泉. 地球科学中同位素体系理论与应用——兼论中国大陆壳幔演化[M]. 北京: 科学出版社, 1998: 1−330.
Zhu Bingquan. The Isotopic System Theory and Application in Earth Science− and on the Crust−Mantle Evolution in China [M]. Beijing: Science Press, 1998: 1−330(in Chinese).

[54] Zartman R E, Doe B R. Plumbotectonics− the model[J]. Tectonophysics, 1981, 75:135−162.